Acta Crystallographica Section D
Biological Crystallography
ISSN 0907-4449

Neutron Laue diffraction studies of coenzyme cob(II)alamin

Paul Langan,[a] Mogens Lehmann,[a] Clive Wilkinson,[b] Gerwald Jogl[c] and Christoph Kratky[c]*

[a]Institut Laue Langevin, BP 156, F-38042 Grenoble CEDEX 9, France, [b]EMBL Outstation, Avenue des Martyrs, F-38042 Grenoble, France, and [c]Department of Structural Biology, Institute of Physical Chemistry, University of Graz, Heinrichstrasse 28, A-8010 Graz, Austria

Correspondence e-mail: christoph.kratky@kfunigraz.ac.at

Received 16 January 1998
Accepted 23 April 1998

Using a recently designed neutron single-crystal diffractometer utilizing a narrow-band Laue concept (LADI), diffraction data were collected from a crystal of the coenzyme cob(II)alamin (B_{12r}), crystallized from a mixture of D_2O and perdeuterated acetone. The instrument was placed at the end of a cold neutron guide at the Institute Laue Langevin (ILL, Grenoble, France), and data collection with neutrons of 1.8–8.0 Å wavelength to a crystallographic resolution of 1.43 Å was complete after about 36 h. This compares favourably with a previous experiment utilizing the same crystal specimen, where more than four weeks were required to collect monochromatic diffraction data to about 1 Å resolution. Using the Laue data, the structure was solved by molecular replacement with the known X-ray crystal structure. Difference density maps revealed the atomic positions (including deuterium atoms) of seven ordered solvent water molecules and two (partially disordered) acetone molecules. These density maps were compared with corresponding maps computed with monochromatic neutron-diffraction data collected to 1.0 Å resolution using the same crystal specimen, as well as to maps derived from high-resolution (0.90 Å) synchrotron X-ray data. In spite of the better definition of atomic positions in the two high-resolution maps, the 1.43 Å LADI maps show considerable power for the determination of the location of hydrogen and deuterium positions.

1. Introduction

The vitamin B_{12} coenzyme (5′-deoxyadenosylcobalamin) is a cofactor of several enzymes catalyzing isomerization *via* a radical mechanism, initiated by homolytic dissociation of the coenzyme's organometallic Co—C bond to generate cob(II)alamin (B_{12r}, Fig. 1) and a 5′-deoxyadenosyl radical (Halpern, 1985). The rate constant of dissociation of the Co—C bond in these reactions is about 10^{10} times that of the free coenzyme, suggesting a weakening of the Co—C bond by interaction with the enzyme in the presence of substrate (Halpern *et al.*, 1984; Finke & Hay, 1984; Hay & Finke, 1986). It has been proposed that this weakening is a result of steric effects (Halpern *et al.*, 1984; Bresciani-Pahor *et al.*, 1985). However, comparison of the crystal structure of B_{12r} (Kräutler *et al.*, 1989) with that of the coenzyme (Lenhert & Hodgkin, 1961; Lenhert, 1968) reveals no major molecular distortion which would explain the observed Co—C bond weakening. It was therefore suggested that the Co—C bond is labilized by way of enzyme-induced separation of the homolysis fragments by strong differential binding of the separated fragments to the enzyme (Kräutler *et al.*, 1989).

The recent elucidation of two crystal structures of proteins or protein subunits containing a B_{12} cofactor has shed new

light upon the role and function of B_{12} cofactors (Ludwig & Matthews, 1997; Kräutler & Kratky, 1996); the crystal structures of both the B_{12}-binding domain of methionine synthase (Drennan *et al.*, 1994) and the complete methylmalonyl CoA mutase (Mancia *et al.*, 1996) revealed the protein-bound B_{12} in a 'base-off' constitution, with a protein-derived imidazole replacing the dimethylbenzimidazole base from its intramolecular cobalt coordination (Ludwig *et al.*, 1996; Padmakumar *et al.*, 1995). While speculations about intramolecular origins for the reactivity enhancement of protein-bound coenzyme B_{12} have thus lost some of their foundation, the mechanism of coenzyme-B_{12}-dependent enzymes as well as the exact role of the B_{12} cofactor are still a matter of dispute (Beatrix *et al.*, 1995; Buckel & Golding, 1996). The crystal structure of methylmalonyl CoA mutase (Mancia *et al.*, 1996) shows an unusually long axial Co—N bond of the B_{12} cofactor [presumably in its Co(II) form], which has again stimulated interest in high-resolution model studies of isolated B_{12} derivatives (Kräutler *et al.*, 1994; Kratky *et al.*, 1995; Gruber *et al.*, 1997).

We are investigating the structure of crystalline coenzyme B_{12r}, the corrinoid product of Co—C bond homolysis of coenzyme B_{12}. The present study is specifically concerned with the solvent structure within B_{12r} crystals. Although X-ray diffraction studies have provided information on solvent structure in crystals of biologically important molecules such as proteins (Edsall & McKenzie, 1983) and nucleic acids (Berman, 1994) very few of these studies achieve the resolution required (<1 Å) to locate weakly scattering H atoms and all solvent atoms. Neutrons offer important advantages for determining solvent structure even at medium resolution, because of the relatively strong scattering power of hydrogen and deuterium, and have been used to investigate the hydration of a number of biological systems (Mason *et al.*, 1984; Teeter & Whitlow, 1986; Wlodawer & Savage, 1989; Forsyth *et al.*, 1989; Langan *et al.*, 1992; Kossiakoff *et al.*, 1992; Deriu *et al.*, 1997; Steiner *et al.*, 1990) including B_{12} (Bouquiere *et al.*, 1993, 1994; Savage, 1986; Savage & Finney, 1986; Savage *et al.*, 1987). However, there have been few of these studies because of the large crystal sizes required to exploit the relatively weak flux of neutron beams and make data collection practicable in a reasonable length of time.

Recently a Laue diffractometer, LADI, has been built at the European Molecular Biology Laboratories (EMBL) outstation in Grenoble which exploits a large image-plate (IP) detector in combination with a Laue neutron beam at the ILL in order to improve data-collection efficiency from such systems (Cipriani *et al.*, 1995, 1996). This paper describes the collection and analysis of data from a B_{12r} crystal at room temperature on LADI over a period of 36 h to 1.43 Å resolution. Results on the identification of the solvent structure as derived from the Laue data are described.

In previous experiments, we have collected neutron-diffraction data from the same crystal specimen on a monochromatic single-crystal neutron diffractometer (station D19 at ILL, Grenoble), where data collection to a resolution of about 1 Å took 28 d (Jogl *et al.*, 1999). Density maps derived from both neutron experiments will also be compared with maps computed from synchrotron X-ray data collected from B_{12r} crystals at room temperature at the EMBL beamline X31 at DESY in Hamburg (Jogl *et al.*, 1999). The present communication describes primarily the results of the LADI experiment, while a detailed description of the high-resolution monochromatic neutron experiment and of the synchrotron X-ray experiment will be published separately (Jogl *et al.*, 1999).

The combined X-ray and neutron-diffraction evidence allows the assessment of the relative merits of X-ray and neutron diffraction for the localization of solvent molecules in a medium-sized model system for a biological macromolecule. Specifically, it demonstrates the performance of the novel LADI diffractometer, which allows the collection of a complete data set to atomic resolution within a few days, almost irrespective of the complexity of the system under investigation. It is envisaged that this instrument will be specifically used in the area of structural biology.

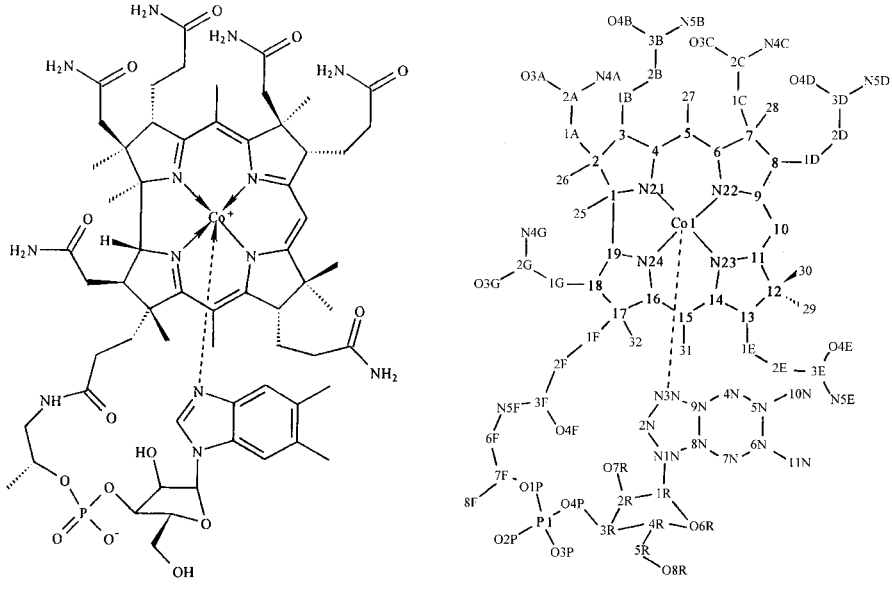

Figure 1
Left: structural formula of cob(II)alamin (B_{12r}). Right: atom numbering used for the description of crystal structures.

2. Experimental methods

2.1. Preparation and crystallization

151.7 mg of hydroxocobalamin–HCl (Fluka) were dissolved in 5 ml H_2O, and a 1.5 molar excess of triethylamine was added. After 2 h, 25 ml acetone was added to the solution and the hydroxocobalamin was left to crystallize at

Table 1
The completeness of the data in resolution shells.

Resolution shell (Å)	3.9	2.8	2.3	2.0	1.8	1.6	1.5	1.42
Total reflections	109	175	213	239	273	304	314	345
Percentage observed	75	94	87	77	72	69	63	38

277 K overnight. Solid hydroxocobalamin was filtered, washed with cold acetone and vacuum dried. 125 mg (82.4%) were recovered and were subsequently dissolved in 5 ml deoxygenated H_2O in a glovebox (Mecaplex, Switzerland; N_2 atmosphere, <15 parts per million O_2). Catalytic reduction was performed with platinum oxide as catalyst at 101 325 Pa H_2 as described in Kräutler *et al.* (1989).

Hexadeuteroacetone and D_2O were used for all following crystallization steps for the neutron experiments. Large crystals of cob(II)alamin were grown in two stages: vapour diffusion (50 ml of an 8.3 mg ml^{-1} solution of B_{12r} in D_2O was equilibrated against 400 ml of deoxygenated d_6-acetone) was used to grow starting crystals that were subsequently used for repeated seeding steps to enlarge crystal size. A starting crystal of typical size 0.6 × 0.4 × 0.3 mm was transferred with an adapted spatula into a wash solution of 60% d_6-acetone in D_2O. After 15 s it was further transferred into a pre-equilibrated solution of cob(II)alamin and left there for further crystal growth.

2.2. Data collection

A 4.5 × 1.4 × 1.3 mm cuboid crystal was held with glass wool in a quartz capillary tube and sealed therein (using epoxy glue) along with its mother liquor. The same crystal specimen was used for both neutron experiments. The crystal within its capillary was mounted on the Laue diffractometer, LADI, built at the European Molecular Biology Laboratory outstation in Grenoble and installed at the high-flux reactor of the Institut Laue Langevin, Grenoble, France. LADI is equipped with a Φ-drive sample holder and a neutron-sensitive image plate, IP, fixed to the exterior of a coaxial cylindrical aluminium drum. The drum is 400 mm in length and 159.2 mm in radius. The IP covers the full length of the drum and 288° of its circumference. The IP is read after exposure by rotating the drum and moving the read head along its length, producing a 4000 × 2000 image with a raster and pixel size of 200 µm. The readout duty cycle is about 8 min.

LADI was positioned at the end of cold neutron guide H142 where the neutron wavelength ranges from 1.8–8 Å. A number of LiF apertures were used to reduce the neutron beam to a circular cross section of 4 mm diameter. The divergence is governed by the guide and varies with wavelength, being about 0.17° Å^{-1}. One of the limitations of Laue geometry for hydrogenous samples is the large wavelength-independent contribution to the background arising from incoherent scattering from hydrogen. Another limitation for samples with large unit cells is the accidental overlap of reflections excited at different wavelengths. In order to minimize both these effects, the wavelength range was reduced by using a Ni/Ti supermirror band-pass filter (Anderson & Hoghoj, 1996). This consisted of about 750 layers of 74–90 Å alternating Ni/Ti laid down on Si substrates. These are stacked side by side and used at grazing incidence. The resulting wavelength distribution was measured by time-of-flight methods to have a peak at 2.8 Å and FWHH of 19%.

The crystal was mounted with its (110) axis approximately parallel to the spindle axis so that most of the unique volume of reciprocal space could be collected by a rotation in φ without having to reset the crystal. φ was moved through 90° in 12 steps of 7.5°, and 3 h exposures were recorded with the crystal stationary at each step. The corresponding images each contained about 1000 spots which were indexed using the program *LAUEGEN* (Collaborative Computational Project, Number 4, 1994). The orientation matrix was refined by least squares, and a satisfactory agreement between observed and predicted spot centres (0.4 mm r.m.s. for a spot size of about 5 × 3 mm) was obtained only when spots corresponding to d spacings of less than 1.4 Å and wavelengths less than 2.5 Å were rejected. This left about 600 spots per image, 7117 in total.

Integration of the reflections was performed by the program *INTEGRATE*, which uses an algorithm based on the $\sigma(I)/I$ method employing an *a priori* knowledge of peak shapes, as described by Wilkinson *et al.* (1988) and by Prince *et al.* (1997). A library of peak shapes generated from 'strong' reflections on the image is used to obtain statistically optimized intensities for weak reflections. The measured intensities were corrected to take account of the wavelength profile of the incident beam using the program *LAUENORM* (Collaborative Computational Project, Number 4, 1994). This program uses equivalent reflections excited by different wavelengths to determine a wavelength-normalization curve which is then applied to the measured intensities. We could not normalize data from different exposures using the same curve because the wavelength profile of the beam had changed over the course of the experiment owing to the influence of other instruments upstream from LADI on H142. The 12 data sets were therefore normalized individually and merged later during structure refinement. Initial $R_{\rm merge}$ values were about 10% for each data set. However, this was reduced to an acceptable level of about 6% by rejecting 1705 reflections at the edges of the wavelength distribution and 376 negative intensities, and using only reflections greater than 3σ to determine the wavelength-normalization curves. This left 4945 reflections, 2158 of which were unique, and after merging the Friedel pairs $-8 \le h \le 5$, $-6 \le k \le 14$, $-18 \le l \le 10$, 1355 reflections remained of which 92% had $F > 4\sigma$. The completeness of the data as a function of resolution is shown in Table 1.

2.3. Structure refinement

The model determined from synchrotron X-ray data collected at room temperature (Jogl *et al.*, 1999) to a resolu-

tion of 0.9 Å from a B_{12r} crystal obtained from H_2O/acetone under otherwise identical conditions to those used in this study was used as our initial phasing model. While we used the atomic coordinates as deduced from the X-ray experiment, the cell dimensions were taken from the high-resolution neutron experiment [Jogl *et al.*, 1999; X-ray cell dimensions: a = 15.996 (5), b = 21.946 (9), c = 26.761 (3) Å; high-resolution neutron cell dimensions: a = 15.987 (1), b = 21.889 (2), c = 26.824 (3) Å]. The parameters of the X-ray model were fixed, while the 12 scaling factors for the neutron data sets were refined using *SHELXL*93 (Sheldrick, 1993), together with a parameter used to model the solvent using Babinet's principle (Langridge *et al.*, 1960), to give an R factor of 24.1%. An $F_o - F_c$ difference map was then calculated and viewed along with the model and peak positions flagged by *SHELXL*93 as being greater than 4σ on an Evans and Sutherland PS300 using the *FRODO* graphics package (Jones, 1978). Seven positive peaks corresponded to density which could be immediately interpreted as D_2O molecules by their shape (Fig. 2). The position and isotropic thermal parameters of the 21 corresponding atoms were refined using blocked least-squares refinement with the internal D—O and D—D distances restrained, reducing the R factor to 19%. The thermal parameters of the three atoms in each molecule were linked to each other by introducing appropriate restraints. A negative density peak covered the D10 hydrogen position on the corrinoid ring, which we had assumed would be totally substituted by deuterium. Allowing the occupancy of this exchange site to refine reduced the R factor to 18.9% and indicated a 70% level of substitution. There was no density at other labile sites to suggest partial exchange and refinement of the extent of their substitution did not significantly improve the R factor.

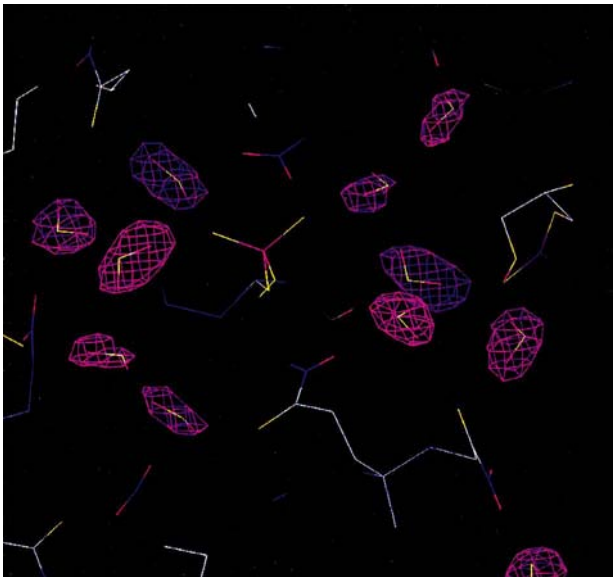

Figure 2
Solvent density, as revealed by the first difference density ($F_o - F_c$) map, computed with phases based on the X-ray crystal structure of B_{12r}. Contouring level is 1.5σ.

Another Fourier difference map was then calculated, this time including the seven water molecules in the F_c and phase calculation, which contained two regions of strong positive density both of which could be interpreted as (perdeuterated) acetone molecules by their shape. These molecules were modelled as rigid bodies with their position and the isotropic temperature parameters of each atom allowed to refine, reducing the R factor further to 17.5%. The thermal parameters of the deuterium atoms on each acetone were constrained to those of covalently bound C atoms.

A further Fourier difference map contained positive density peaks in the large solvent channel which could not be interpreted easily as further ordered water or acetone molecules. However, density around some of the amide and hydroxyl groups suggested that the agreement of the X-ray model with the neutron data could be improved by allowing the orientation of these groups to refine. Allowing the position of all deuterium atoms on the B_{12r} molecule to refine while

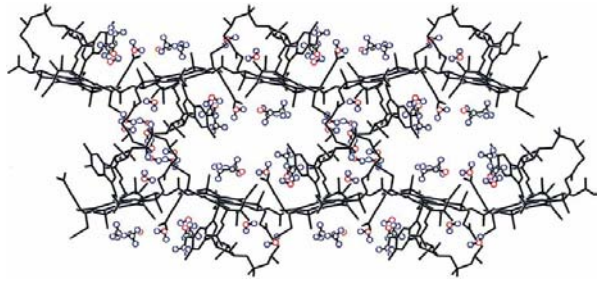

Figure 3
Projection of the crystal structure of cob(II)alamin along the crystallographic a axis.

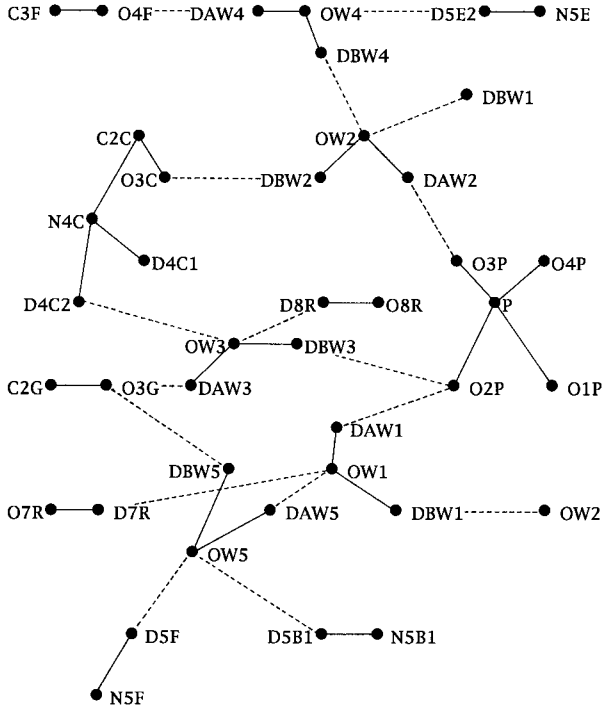

Figure 4
The solvent network involving water molecules W1 to W5.

Table 2
Fractional atomic coordinates and isotropic displacement parameters (U values) for the atoms of the seven water and two acetone molecules.

	x	y	z	U
OW1	0.7614 (24)	0.2618 (18)	0.4693(14	0.091 (14)
DAW1	0.7030 (27)	0.2627 (19)	0.4626 (13)	0.136
DBW1	0.7717 (27)	0.2574 (17)	0.5041 (16)	0.136
OW2	0.2224 (19)	0.7379 (18)	0.9253 (13)	0.073 (12)
DAW2	0.1705 (25)	0.7580 (13)	0.9308 (13)	0.110
DBW2	0.2119 (26)	0.6957 (16)	0.9200 (13)	0.110
OW3	0.1084 (24)	0.1307 (17)	0.5849 (14)	0.075 (13)
DAW3	0.1483 (27)	0.1208 (14)	0.6101 (15)	0.112
DBW3	0.1144 (27)	0.1723 (18)	0.5757 (13)	0.112
OW4	0.6661 (37)	0.2698 (22)	0.6605 (19)	0.153 (19)
DAW4	0.6539 (40)	0.2274 (25)	0.6614 (22)	0.230
DBW4	0.7121 (37)	0.2778 (24)	0.6390 (25)	0.230
OW5	0.3283 (24)	0.1375 (24)	0.5469 (20)	0.136 (17)
DAW5	0.2845 (36)	0.1667 (23)	0.5439 (21)	0.203
DBW5	0.3095 (41)	0.1032 (21)	0.5653 (20)	0.203
OW6	0.1503 (39)	0.0532 (25)	0.8252 (13)	0.131 (18)
DAW6	0.1260 (42)	0.0899 (24)	0.8376 (21)	0.197
DBW6	0.1612 (41)	0.0258 (22)	0.8518 (22)	0.197
OW7	0.1107 (57)	0.1766 (39)	0.8695 (21)	0.226 (29)
DAW7	0.0926 (63)	0.1674 (48)	0.9023 (33)	0.338
DBW7	0.1556 (58)	0.2050 (51)	0.8705 (34)	0.338
C1A2	0.5146 (30)	0.5758 (24)	0.5649 (15)	0.342 (32)
D1A2A	0.5391 (38)	0.5456 (31)	0.5430 (15)	0.513
D1A2B	0.5260 (39)	0.6163 (28)	0.5520 (19)	0.513
D1A2C	0.4548 (30)	0.5696 (30)	0.5667 (21)	0.513
C2A2	0.5518 (26)	0.5697 (14)	0.6160 (14)	0.255 (25)
C3A2	0.6421 (27)	0.5513 (26)	0.6183 (18)	0.354 (31)
D3A2A	0.6747 (26)	0.5777 (35)	0.5968 (23)	0.530
D3A2B	0.6479 (37)	0.5094 (28)	0.6073 (23)	0.530
D3A2C	0.6620 (34)	0.5550 (32)	0.6522 (20)	0.530
O4A2	0.5096 (34)	0.5742 (26)	0.6532 (15)	0.222 (27)
C5A1	0.2240 (90)	0.3953 (30)	0.8885 (51)	1.034 (46)
D5A11	0.2487 (116)	0.4163 (43)	0.8607 (60)	1.550
D5A12	0.2486 (111)	0.4098 (51)	0.9190 (56)	1.550
D5A13	0.1649 (96)	0.4029 (28)	0.8891 (70)	1.550
C6A1	0.2392 (43)	0.3283 (35)	0.8836 (24)	1.000 (47)
C7A1	0.3287 (40)	0.3079 (75)	0.8865 (70)	1.211 (47)
D7A11	0.3492 (68)	0.3139 (90)	0.9197 (78)	1.817
D7A12	0.3618 (54)	0.3314 (93)	0.8636 (81)	1.817
D7A13	0.3323 (58)	0.2654 (77)	0.8779 (87)	1.817
O8A1	0.1833 (44)	0.2932 (24)	0.8736 (19)	0.177 (22)

restraining their bond lengths further reduced the R factor to 16.2%.

Allowing the position and orientation of the corrinoid ring, the phosphate group and the benzimidazole group to refine as rigid bodies and the side chains to refine in a torsionally restrained manner further reduced the R factor to 15.7% without introducing too many additional parameters (in total 982 parameters and 966 restraints). However, although the geometry of the model changed little, it is difficult to justify refinement of a highly accurate X-ray model against neutron data to a lower resolution, and we did not consider it to be a significant improvement. Allowing the occupancy of the water or acetone molecules to refine or introducing anisotropic atomic displacement parameters did not significantly improve the R factor. However, it did indicate that the acetone molecule which lies above the Co atom is probably disordered. The resultant values of the parameters of this refinement are represented in Table 2 for the atoms of the nine water and two acetone molecules.

3. Results

3.1. Solvent structure

The molecular structure of B_{12r} has been described (Kräutler *et al.*, 1989) and we retain their system for assigning atom labels. We refer to the benzimidazole side of the molecule as its bottom. From Fig. 3, which shows a view of the crystal structure projected down the *a* axis, it can be seen that the molecules lie in corrugated planes with the repeat motif being a strip of molecules pointing up next to a strip pointing down. Corrugated planes are stacked so that charged phosphate groups from opposing molecules in neighbouring planes interdigitate, thus forming a relatively compact column of charged groups running along the *a* direction. Water molecules W1 to W5, represented in Fig. 4, are located in this region and make most of the links between the stacked planes. These five water molecules have D atoms which hydrogen bond to an O atom (four to amides, three to phosphates, three to waters) and O atoms which participate in two hydrogen bonds, except W5 which seems to participate in only one (three to water, four to amides, two to hydroxyls). W1, W3, W4 and W5 are hydrogen bonded to each other forming single, double, triple and quadruple water bridges between the various B_{12r} groups in this hydrophilic region.

A large open solvent channel is present along the *a*-axis direction with the relatively hydrophobic corrin and benzimidazole fragments forming its walls (Hohenester *et al.*, 1991). The two acetone molecules A1 and A2 and water molecules W6 and W7 represented in Fig. 5 are located in this region and constitute an ordered solvent shell which lines the channel. W6 and W7 form a double-water bridge between the amide groups of the acetamide ligands *A* and *B* of the same molecule. W7 also forms a hydrogen bond to an O atom of an amide group of a neighbouring molecule. W6 forms a hydrogen bond to the O atom of A1. This double-water bridge therefore seems to anchor A1 over the corrin fragment. The oxygen of A2 hydrogen bonds to the amide of a propionamide group, anchoring it over the benzimidazole fragment.

3.2. Hydrogen-bonding geometries

The hydrogen-bonding geometries involving solvent molecules are represented in Table 3 and those involving only B_{12r} atoms in Table 4. The covalent bond lengths and angles of the water molecules were tightly restrained during refinement.

Table 3
Hydrogen-bond geometries involving solvent molecules.

X represents either the B_{12r} or solvent donor atom. E.s.d.s are given in parentheses in units of the last digit.

	X—D (Å)	*X*—O (Å)	D···O (Å)	*X*—D···O (°)
B_{12r} donors				
N5E—D5E2···OW4	0.977	2.956 (54)	1.982 (54)	174 (2)
N4C—D4C2···OW3	0.982	2.946 (40)	2.067 (39)	148 (1)
O7R—D7R···OW1	0.940	2.844 (34)	1.909 (34)	173 (1)
N5F—D5F···OW5	0.887	2.928 (49)	2.047 (49)	172 (1)
N5B—D5B1···OW5	1.033	3.187 (49)	2.419 (51)	130 (1)
O8R—D8R···OW3	0.954	2.942 (37)	2.007 (38)	166 (1)
N4G—D4G2···OW7	0.979	2.943 (34)	2.943 (35)	174 (2)
N4A—D4A2···OW6	0.965	3.184 (91)	2.228 (89)	171 (2)
N5D—D5D2···O4A2	0.991	3.060 (54)	2.111 (54)	160 (1)
Water donors				
OW1—DAW1···O2P	0.951 (11)	2.706 (40)	1.758 (42)	175 (4)
OW1—DBW1···O2L	0.951 (11)	2.885 (53)	1.943 (56)	156 (3)
OW2—DBW2···O3CO	0.951 (10)	2.516 (40)	1.593 (35)	162 (4)
OW2—DAW2···O3P	0.951 (10)	2.721 (34)	1.823 (40)	156 (3)
OW3—DAW3···O3G	0.955 (10)	2.836 (38)	1.891 (40)	170 (5)
OW3—DBW3···O2P	0.948 (10)	2.617 (42)	1.712 (35)	158 (4)
OW4—DAW4···O4F	0.949 (11)	2.583 (60)	1.770 (52)	142 (7)
OW4—DBW4···OW2	0.950 (11)	2.993 (53)	2.199 (70)	140 (5)
OW5—DAW5···OW1	0.950 (8)	2.488 (62)	1.647 (53)	145 (6)
OW5—DBW5···O3G	0.948 (10)	3.213 (44)	2.566 (56)	126 (6)
OW7—DAW7···OW6	0.952 (11)	3.018 (97)	2.096 (97)	166 (7)
OW7—DBW7···O4B	0.947 (11)	2.515 (52)	1.586 (51)	163 (8)
OW6—DBW6···O8A1	0.950 (11)	2.805 (91)	1.981 (110)	144 (14)

Table 4
B_{12r} intermolecular hydrogen-bond geometries.

X represents either the B_{12r} or solvent donor atom.

	X—D (Å)	*X*—O (Å)	D···O (Å)	*X*—D···O (°)
N4C—D4C1···O3P	1.031	3.029	2.013	167.77
N4A—D4A1···O4D	1.038	3.038	2.010	170.55
N5B—D5B2···O3P	0.978	2.997	2.038	166.09
N5E—D5E1···O3A	1.026	2.878	1.997	142.36
N4G—D4G1···O4E	1.023	2.982	2.096	143.53

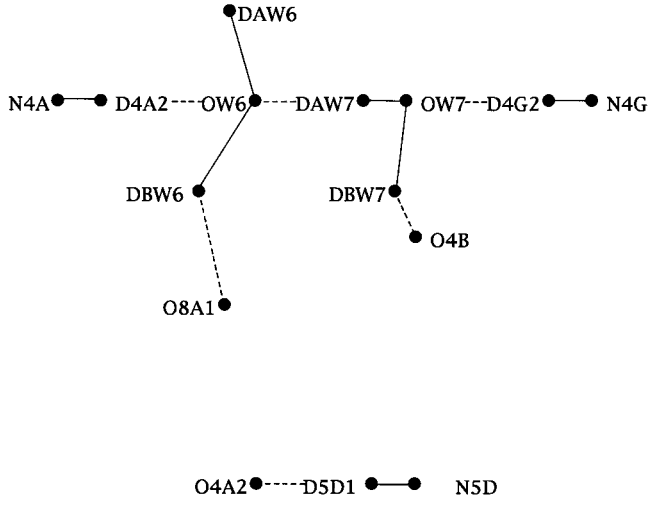

Figure 5
The solvent network involving solvent water molecules W6 and W7 and the two acetone molecules A1 and A2.

The hydrogen-bond distances made by water oxygen acceptors range from 2.49 to 3.19 Å with a mean value of 2.94 Å. This compares to a mean value of 2.88 Å for the coenzyme at 15 K (Bouquiere *et al.*, 1994). The hydrogen-bond lengths made by water D atoms range from 1.59 to 2.57 Å with a mean value of 1.99 Å. This compares to a mean value of 1.95 Å for the coenzyme at 15 K. The angles made by water hydrogen-bond donors vary from 126 to 175° with a mean value of 154°, compared to a mean value of 161° for the coenzyme at 15 K.

4. Discussion

4.1. Solvent structure in B_{12r} crystals

All the highly ordered water molecules W1 to W5 in the hydrophilic region at the interface between stacked planes of molecules are involved in bridges to the charged phosphate groups. This network of water mediates the interaction of the phosphate groups with their surrounding environment. All the hydrogen-bonding donor potential of these five water molecules is used, with the range of hydrogen-bond lengths and angles similar to those observed in small hydrate structures and the B_{12} coenzyme. 90% of the hydrogen-bonding acceptor potential is used (assuming a potential of two hydrogen bonds per water lone-pair region). Only two direct hydrogen bonds are made between a phosphate and a B_{12r} group from a neighbouring molecule.

This contrasts with the situation in crystals of the coenzyme B_{12} (Bouquiere *et al.*, 1994) where the phosphate groups make three direct hydrogen bonds with groups from neighbouring molecules and fewer bonds through water. The difference in phosphodiester conformation between B_{12r} and the coenzyme is due to the different crystal environment of the charged phosphates and their interaction with this environment through water and hydrogen bonding.

The role of the two ordered water and acetone molecules in the large solvent channel appears to be less crucial, interfacing the fairly hydrophobic walls of this channel with the disordered solvent inside. In crystals of the coenzyme such a channel does not exist, the top of the molecules being occupied by AdCH2 which hydrogen bonds with the phosphate groups on the down side of molecules in neighbouring planes. In this study we have not attempted to investigate the more disorded solvent molecules in this channel, which will be analyzed in more detail in our report of the neutron-diffraction studies on the high-resolution diffractometer D19 at the ILL (Jogl *et al.*, 1999).

4.2. Neutron Laue diffraction

Compared to the classical collection of monochromatic neutron data (*e.g.* at ILL station D19), use of the novel LADI instrument enhances the speed of neutron data collection by more than one order of magnitude. However, the price to be paid is a decrease in resolution (for the present project 1.43 Å *versus* 1.0 Å) and a worse signal-to-noise ratio. In the design of the LADI instrument, these drawbacks were considerd acceptable in view of the prospective use of LADI for the investigation of protein crystals, whose diffraction rarely extends beyond 1.4 Å. In order to assess the effect of the differences in technical specifications (such as the resolution limit, which arises from the size of the image plate and the available wavelength band) and to appraise the utility of the novel LADI instrument, we have calculated density maps for selected regions of the B_{12r} crystal structure. A comparison is made between maps obtained from synchrotron X-ray data (resolution 0.9 Å), from monochromatic neutron data (reso-

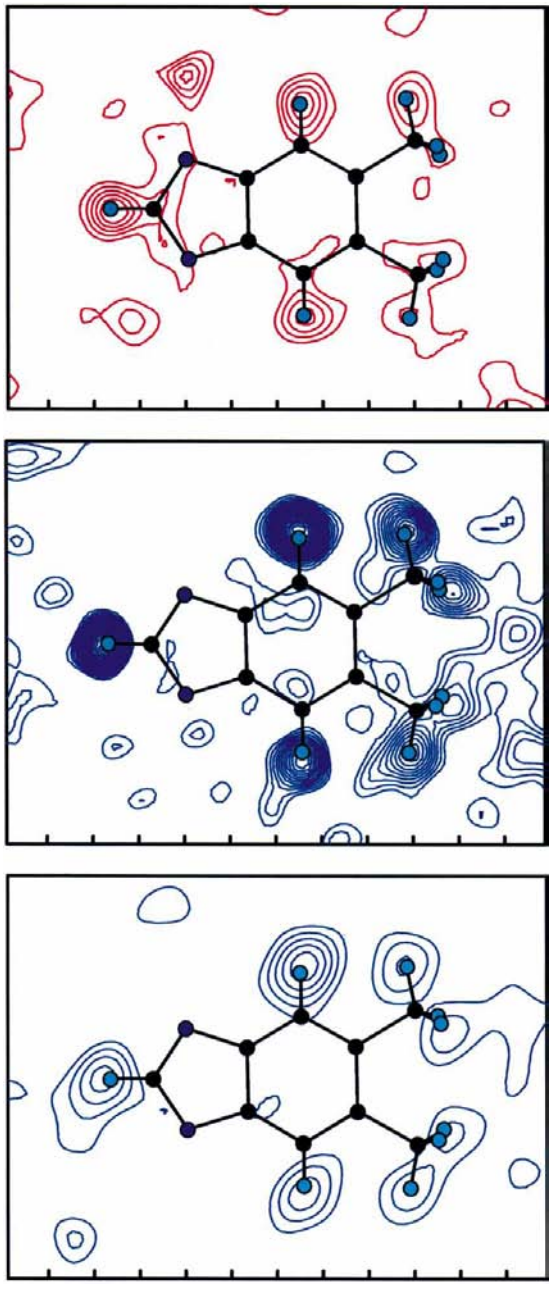

Figure 6
Difference-density omit maps for the crystal structure of cob(II)alamin computed from synchrotron X-ray data (0.9 Å resolution, top), monochromatic neutron-diffraction data (1.0 Å resolution, centre) and incomplete (see Table 1) neutron Laue-diffraction data (1.43 Å resolution, bottom). The map was computed for a plane passing through the non-H atoms of the dimethylbenzimidazole base, after omitting its three H atoms. Contouring started at a significance level of $\pm 1\sigma$, with 1σ difference between subsequent contour lines. Negative contours are represented in blue and positive contours in red.

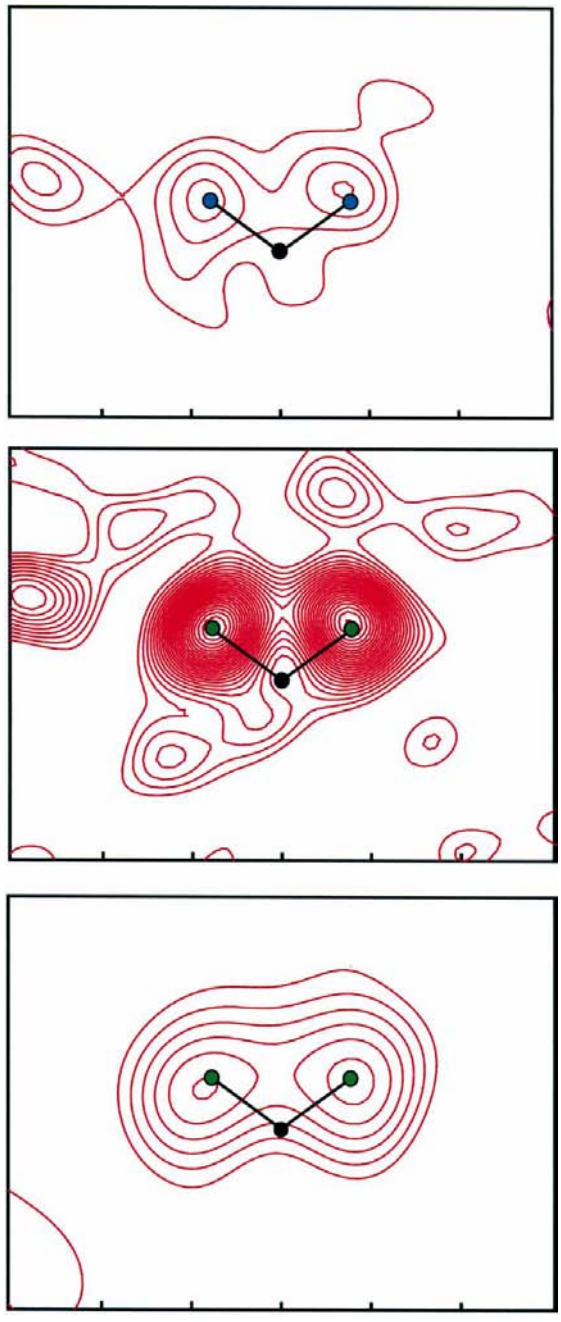

Figure 7
Omit maps (see legend to Fig. 6) through the atoms of water molecule W1. The two H or D atoms have been omitted for the phase calculation.

lution 1.0 Å) and from the (incomplete) 1.43 Å LADI data collected with the same crystal specimen as the monochromatic neutron data.

Fig. 6 shows a density section through the dimethylbenzimidazole (DMB) ring, prototypical for the very well ordered parts of the structure. Difference densities are calculated for the least-squares plane through all C and N atoms of the DMB moiety, and the H (or D) atoms at positions 2, 4 and 7 have been omitted for the calculation of phases. All three maps are contoured at the same level of significance. Evidently, each of the three omit-maps clearly reveal the positions of the H atoms. Not surprisingly, the monochromatic 1.0 Å neutron data show the H-atom positions (which appear as negative peaks in the two neutron maps) with highest significance. However, when comparing the difference maps computed with the (incomplete) 1.43 Å LADI data with the 0.9 Å X-ray data, it is remarkable that the neutron data led to a map of at least the same quality as the X-ray data, in spite of the latter's far better resolution, completeness and statistical significance.

This picture is corroborated by Fig. 7, which shows a corresponding set of maps through the three atoms of water (or D_2O) molecule W1. The figure shows omit-maps for the two H or D atoms. Again, the monochromatic neutron map is outstanding, with the LADI map being second with respect to its ability to reveal hydrogen or deuterium positions.

Finally, as a reference, we show a section through the acetone molecule A1 in Fig. 8. Here, all atoms (C, O and H or D) of the solvent molecule have been omitted when computing phases for the difference densities. While the superior quality of the synchrotron X-ray data for locating non-H atoms is quite evident, both neutron maps also indicate the deuteration of the two methyl groups, in spite of their torsional disorder.

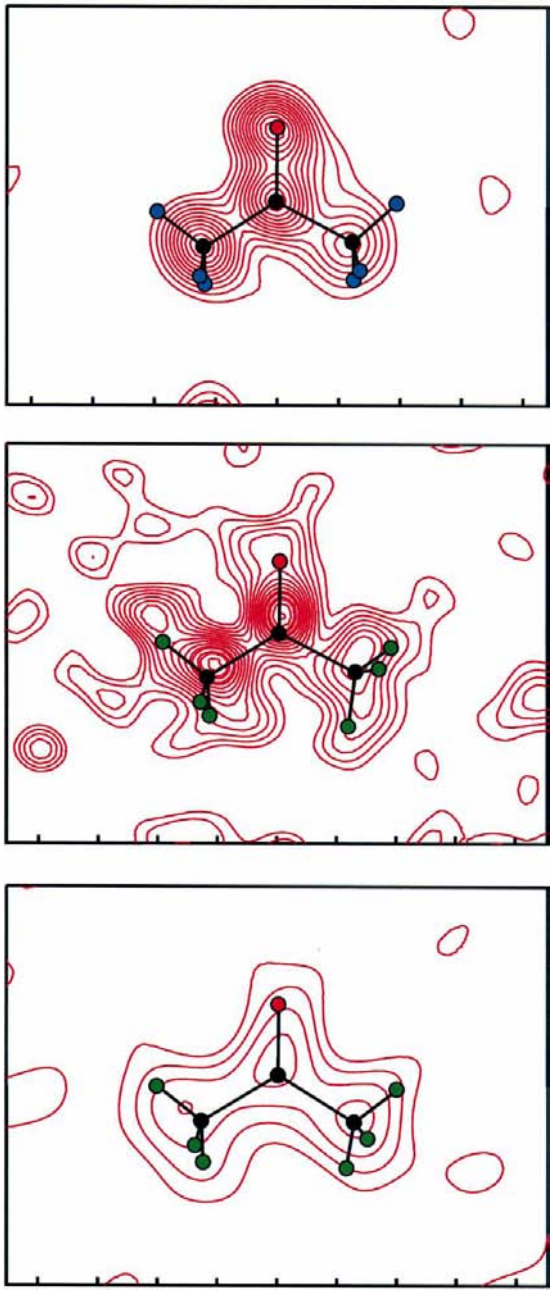

Figure 8
Omit-maps (see legend to Fig. 6) through the non-H (or non-D) atoms of acetone molecule A1. All atoms of this solvent molecule have been omitted for the calculation of phases.

5. Conclusions

High-resolution high-accuracy neutron measurements on biological crystals still require long data-collection periods of at least several weeks on classical single-wavelength diffractometers (such as D19) at ILL. However, as this study shows, the gains in data-collection efficiency using a Laue approach open up the possibility of rapid data collection at medium resolution, where density maps of excellent quality with a high power for locating H or D atoms can still be obtained. Perhaps more significantly, availability of the novel LADI instrument will allow data collection from smaller crystals and, therefore, a wider range of systems to become practicable.

We thank the ILL and the EMBL for the provision of facilities. The synchrotron X-ray data were collected at the EMBL beamline X31 at DESY in Hamburg. We thank Z. Dauter and K. Wilson for their help. This research was supported in part by the Austrian Fonds zur Förderung der wissenschaftlichen Forschung (projects P-9542 and P-11599).

References

Anderson, I. & Hoghoj, P. (1996). Annual Report Insititut Laue Langevin, pp. 84–85. Insititut Laue Langevin, Grenoble, France.
Beatrix, B., Zelder, O., Kroll, F. K., Örlygsson, G., Golding, B. T. & Buckel, W. (1995). *Angew. Chem. Int. Ed. Engl.* **34**, 2398–2401.
Berman, H. M. (1994). *Curr. Opin. Struct. Biol.* **4**, 345–350.
Bouquiere, J. P., Finney, J. L., Lehmann, M. S., Lindley, P. F. & Savage, H. F. J. (1993). *Acta Cryst.* B**49**, 79–89.
Bouquiere, J. P., Finney, J. L. & Savage, H. F. J. (1994). *Acta Cryst.* B**50**, 566–578.
Bresciani-Pahor, N., Forcolin, M., Toscano, P. J., Summers, M. F., Randaccio, L. & Marzilli, L. G. (1985). *Coord. Chem. Rev.* **63**, 1–125.
Buckel, W. & Golding, B. T. (1996). *Chem. Soc. Rev.* pp. 329–337.
Cipriani, F., Castagna, J.-C., Lehmann, M. S. & Wilkinson, C. (1995). *Physica B*, **213/214**, 975–979.

Cipriani, F., Castagna, J.-C., Wilkinson, C., Oleinek, P. & Lehmann, M. S. (1996). *J. Neutron Res.* **4**, 79–85.
Collaborative Computational Project, Number 4 (1994). *Acta Cryst.* D**50**, 760–763.
Deriu, A., Cavatorta, F., De Micheli, T., Rupprecht, A. & Langan, P. (1997). *Physica B*, **234/235**, 215–216.
Drennan, L. C., Huang, S., Drummond, J. T., Matthews, R. G. & Ludwig, M. L. (1994). *Science*, **266**, 1669–1674.
Edsall, J. T. & McKenzie, H. A. (1983). *Adv. Biophys.* **16**, 55–183.
Finke, R. G. & Hay, B. P. (1984). *Inorg. Chem.* **23**, 3041–3043.
Forsyth, V. T., Mahendrasingam, A., Pigram, W. J., Greenall, R. J., Bellamy, K., Fuller, W. & Mason, S. A. (1989). *Int. J. Biol. Macromol.* **11**, 236–239.
Gruber, G., Jogl, G., Klintschar, G. & Kratky, C. (1997). In *Vitamin B_{12} and B_{12} Proteins*, edited by B. Kräutler & B. T. Golding. Weinheim: Verlag Chemie.
Halpern, J. (1985). *Science*, **277**, 869–875.
Halpern, J., Kim, S.-H. & Leung, T. W. (1984). *J. Am. Chem. Soc.* **106**, 8317–8319.
Hay, B. P. & Finke, R. G. (1986). *J. Am. Chem. Soc.* **108**, 4820–4829.
Hohenester, E., Kratky, C. & Kräutler, B. (1991). *J. Am. Chem. Soc.* **113**, 4523–4530.
Jogl, G., Langan, P. & Kratky, C. (1999). In preparation.
Jones, T. A. (1978). *J. Appl. Cryst.* **11**, 265–272.
Kossiakoff, A. A., Sintchak, M. D., Shpungin, J. & Presta, L. G. (1992). *Proteins Struct. Funct. Genet.* **12**, 223–236.
Kratky, C., Färber, G., Gruber, K., Wilson, K., Dauter, Z., Nolting, H. F., Konrat, R. & Kräutler, B. (1995). *J. Am. Chem. Soc.* **117**, 4654–4670.
Kräutler, B., Keller, W. & Kratky, C. (1989). *J. Am. Chem. Soc.* **111**, 8936–8938.
Kräutler, B., Konrat, R., Stupperich, E., Färber, G., Gruber, K. & Kratky, C. (1994). *Inorg. Chem.* **33**, 4128–4139.
Kräutler, B. & Kratky, C. (1996). *Angew. Chem. Int. Ed. Engl.* **35**, 167–170.
Langan, P., Forsyth, V. T., Mahendrasingam, A., Pigram, W. J., Mason, S. A. & Fuller, W. (1992). *J. Biomol. Struct. Dyn.* **10**, 489–503.
Langridge, R., Marvin, D. A., Seeds, W. E., Wilson, H. R., Hooper, C. W., Wilkins, M. H. F. & Hamilton, L. D. (1960). *J. Mol. Biol.* **2**, 38–64.
Lenhert, P. G. (1968). *Proc. R. Soc. London Ser. A*, **303**, 45–84.
Lenhert, P. G. & Hodgkin, D. C. (1961). *Nature (London)* **192**, 937–938.
Ludwig, M. L., Drennan, C. L. & Matthews, R. G. (1996). *Structure*, **4**, 505–512.
Ludwig, M. L. & Matthews, R. G. (1997). *Annu. Rev. Biochem.* **66**, 269–313.
Mancia, F., Keep, N. H., Nakagawa, A., Leadlay, P. F., McSweeney, S., Rasmussen, B., Bösecke, P., Diat, O. & Evans, P. (1996). *Structure*, **4**, 339–350.
Mason, S. A., Bentley, G. A. & McIntyre, G. J. (1984). *Neutrons in Biology*, edited by B. P. Schoenborn, pp. 323–334. New York: Plenum Press.
Padmakumar, R., Taoka, S., Padmakumar, R. & Banerjee, R. (1995). *J. Am. Chem. Soc.* **117**, 7033–7034.
Prince, E., Wilkinson, C. & McIntyre, G. J. (1997). *J. Appl. Cryst.* **30**, 133–137.
Savage, H. F. J. (1986). *Biophys. J.* **50**, 947–980.
Savage, H. F. J. & Finney, J. L. (1986). *Nature (London)* **322**, 717–720.
Savage, H. F. J., Lindley, P. F., Finney, J. L. & Timmins, P. A. (1987). *Acta Cryst.* B**43**, 280–295.
Sheldrick, G. M. (1993). *SHELXL93, a Program for the Refinement of Single-Crystal Diffraction Data.* University of Gottingen, Germany.
Steiner, T., Mason, S. A. & Saenger, W. (1990). *J. Am. Chem. Soc.* **112**, 6184–6190.
Teeter, M. M. & Whitlow, M. D. (1986). *Trans. Am. Crystallogr. Assoc.* **22**, 75–88.
Wilkinson, C., Khamis, H. W., Stansfield, R. F. D. & McIntyre, G. J. (1988). *J. Appl. Cryst.* **21**, 471–478.
Wlodawer, A. & Savage, H. (1989). *Acta Cryst.* B**45**, 99–107.